

# Post-Ore Processes of Uranium Migration in the Sandstone-Hosted Type Deposits: $^{234}\text{U}/^{238}\text{U}$ , $^{238}\text{U}/^{235}\text{U}$ and U–Pb Systematics of Ores of the Namaru Deposit, Vitim District, Northern Transbaikalia

V. N. Golubev<sup>a, \*</sup>, N. N. Tarasov<sup>a</sup>, I. V. Chernyshev<sup>a</sup>, A. V. Chugaev<sup>a</sup>, G. V. Ochirova<sup>a</sup>, and B. T. Kochkin<sup>a</sup>

<sup>a</sup> *Institute of Geology of Ore Deposits, Petrography, Mineralogy and Geochemistry,  
Russian Academy of Sciences, Moscow, 119017 Russia*

\*e-mail: golub238@gmail.com

Received July 20, 2020; revised April 15, 2021; accepted April 23, 2021

**Abstract**—To assess the nature of the post-ore behaviour of uranium in the Namaru deposit (Khiagda ore field), U–Pb isotope systems and the isotopic composition of uranium ( $^{234}\text{U}/^{238}\text{U}$  and  $^{238}\text{U}/^{235}\text{U}$ ) were studied. The studied samples represent different ore zones of the deposit and were collected along cross-sections both vertically and horizontally. Wide variations in the isotopic composition of uranium and U–Pb isotopic age have been established. Deviations of the  $^{234}\text{U}/^{238}\text{U}$  ratio from equilibrium values, which for some samples exceed 50%, along with significant variations in the isotopic age, indicate that permafrost layer, which covered the catchment areas of paleovalleys with meteoric oxygen-containing waters ca. 2.5 Ma ago, did not lead to preserving uranium ores at the deposit. Uranium migration took place during the Quaternary period. The effective combining the U–Pb dating and  $^{234}\text{U}/^{238}\text{U}$  data in assessing the post-ore redistribution of uranium made it possible to recognize: removal of uranium from some zones of the ore body and its accompanying redeposition in others. Wide variations in the  $^{238}\text{U}/^{235}\text{U}$  (137.484–137.851) ratios throughout the entire studied cross-sections can be explained by the different locations of samples relatively to the ore deposition front and change in redox conditions as this front advanced. Depletion of the light isotope  $^{235}\text{U}$  in the lower zone of the ore body may be associated with the influence of ascending carbonic waters established in the regional basement. The effect of such waters on uranium-bearing rocks causes predominant leaching of light  $^{235}\text{U}$ .

**Keywords:** sandstone-type uranium deposits, U–Pb age, U isotopic composition, isotope fractionation of  $^{238}\text{U}$  and  $^{235}\text{U}$ , U post-ore redistribution

**DOI:** 10.1134/S1075701521040024

## INTRODUCTION

Interest in studying the formation conditions of ore concentrations of sandstone-type deposits has increased because uranium deposits belonging to the economic sandstone type account for about 30% of global uranium resources (Cuney and Kyser, 2008) and 53% of global mining (Zhivov et al., 2012). In recent years, the share of these deposits in the total base of uranium raw materials in the Russian Federation has significantly increased, currently amounting to at least 38% (Svyatetsky et al., 2017). These deposits are formed in permeable (sandstones, gravelites, unsorted sand-gravel mix) layers of sedimentary rocks, in depressions (foothill, intermontane, valley), due to the infiltration of groundwater through them. Oxygen-saturated atmospheric waters leach uranium dispersed in the rocks. The uranium, when entering the deep horizons of sedimentary rocks of these basins, is deposited at reducing barriers along the boundary of the oxidation zone from the side of initially gray-colored rocks.

The sandstone-type deposits known in the world are located in different climatic zones. Climatic factor controls the behavior of uranium in redox processes and the formation and subsequent change in ore concentrations. The deposits of the Vitim uranium ore district (VUD)—one of the main uranium ore districts in Russia. In contrast to most other sandstone-type deposits located mainly in temperate and warm climate, VUD is in a permafrost zone. It is believed that the permafrost prevents the migration of meteoric oxygen-containing waters over long time periods in sequences with uranium mineralization. This largely determines the views on the features in the behavior of uranium at the VUD deposits.

Recently, starting with (Stirling et al., 2007), it became possible to study natural variations in the isotope ratio  $^{238}\text{U}/^{235}\text{U}$ . In a recent review (Andersen et al., 2017), numerous summarized determinations of this ratio in various natural environments have shown that  $^{238}\text{U}/^{235}\text{U}$  data can be used as information about

the formation processes of natural objects. The study of  $^{238}\text{U}/^{235}\text{U}$  variations in sandstone-type uranium deposits has made it possible to conclude that a change in redox conditions with the successive advancement of the uranium deposition front causes significant fractionation of  $^{238}\text{U}$  and  $^{235}\text{U}$ , both in the uranium ores themselves (Golubev et al., 2013; Murphy et al., 2014) and in migrating waters in ore-hosting rocks (Murphy et al., 2014; Basu et al., 2015; Placzek et al., 2016). These studies contributed additional information on the formation conditions of sandstone-type uranium deposits.

Golubev et al. (2013), in studying the U–Pb isotope systems and isotopic composition of uranium samples from a borehole drilled in the productive sequence of the Dybyn uranium deposit in the Khiagda ore field (KhOF) of the VUD, demonstrated the possibility of using these data to assessing the post-ore redistribution of uranium. This paper presents the results of studying the U–Pb isotope systems and isotopic composition of uranium ( $^{234}\text{U}/^{238}\text{U}$  and  $^{238}\text{U}/^{235}\text{U}$ ) of a set of samples collected in different zones of a cross section through ore body no. 5 of the Namaru uranium deposit in the KhOF. This study, carried out at the Laboratory of Isotope Geochemistry and Geochronology of IGEM RAS, was aimed at obtaining data to assess the behavior of uranium in this ore body by examining different areas of its vertical and cross sections. In addition to the new approach in study of the distribution of the  $^{238}\text{U}/^{235}\text{U}$  ratio, we used a method that is traditional in studying exogenic uranium deposits: analysis of variations in the  $^{234}\text{U}/^{238}\text{U}$  ratio caused by a shift in the  $^{234}\text{U}$  content with respect to the equilibrium  $^{234}\text{U}/^{238}\text{U}$  ratio.

## GEOLOGY OF THE DEPOSIT

The Namaru deposit is located on the southern flank of the Amalat plateau in the northwestern part of the KhOF. The deposit belongs to the paleovalley sub-type or paleovalley sandstone-hosted economic type (Mashkovtsev et al., 2010), which constitutes the main potential of uranium at the VUD. The deposit contains six NW-trending paleovalleys that are part of the Atalanga River paleosystem. The valleys extend to a distance of 3–5 km, with a width of 400–700 m in the upper reaches to 1300 m at confluence points. All the paleovalleys are V-shaped in cross section, with slope angles from  $15^\circ$  to  $25^\circ$ . The host rocks at the deposit are terrigenous-volcanic rocks of the Dzhilinda Formation ( $N_1dz$ ), overlying basement consisting mainly of granites of the Vitimkan Complex ( $\gamma\text{PZ}_1v$ ). The thickness of the terrigenous sequence that makes up the lower part of the formation (almost all ore bodies of the deposit are concentrated in it) sharply changes from a few meters in the upper reaches of the paleoval-

leys to 40–50 m in their lower reaches. The rocks in the upper part of the Dzhilinda Formation are represented by various mafic rocks. The uppermost parts are basalt flows. The total thickness of the volcanosedimentary part of the formation reaches 200–240 m (Mashkovtsev et al., 2010).

The ore-controlling oxidation zoning of the KhOF deposits has been almost completely transformed by secondary reduction processes. The modern hydrochemical conditions in the ore bodies of the KhOF fundamentally differ from those typically to classical hydrogenous deposits. These features are associated with the limited (ceased) infiltration of oxygen-rich uranium-bearing waters into the ore-bearing medium during ongoing reduction processes. The limit of the inflow of meteoric waters into the ore body is associated with the following processes: (1) the terrigenous sequence overlain by basalts; (2) the development of a permafrost layer (average thickness of about 72 m), which began to form about 2.5 Ma ago and completely covers the catchment area of the paleovalley system; (3) inflow of reducing waters through fault zones from the basement (Mashkovtsev et al., 2010; Kochkin et al., 2014); inflow sources of cold carbonic water with  $\text{pH} \sim 5$  in the ore-bearing horizons (Kochkin et al., 2017a). Taking into account these features of the KhOF, two stages are distinguished in the development of its ore-forming system: the first is infiltration ore formation with the involvement of meteoric oxygen-containing waters; the second is conservation of uranium ores (Kochkin et al. 2017b).

Uranium mineralization at the Namaru deposit is represented by a mineral close in composition to ningyoite–Ca-phosphate of tetravalent uranium. Under a microscope, it is observed as fine (usually no more than 5  $\mu\text{m}$ ), irregularly shaped segregations or crustlike formations around detrital material of the host rocks. Some areas concentrate segregations of this mineral with various morphologies (Fig. 1).

## ANALYTICAL METHODS

Taking into account the predominantly finely dispersed character of the uranium mineralization, the U–Pb isotope systems and isotopic composition of uranium were studied using whole-rock samples characterizing different parts of the ore intervals of the studied boreholes. For this, we used quartered the core samples. The chemical composition of all samples was studied. The analysis was performed by X-ray fluorescence spectrometry on a Philips PW2400 sequential spectrometer (analyst A.I. Yakushev, IGEM RAS). When calibrating the spectrometer, industrial and state standard samples of the chemical composition of the mineral raw materials were used. The  $\text{Fe}_2\text{O}_3$  and FeO contents were determined by the traditional chemical method (analyst S.I. Kogan, IGEM RAS).

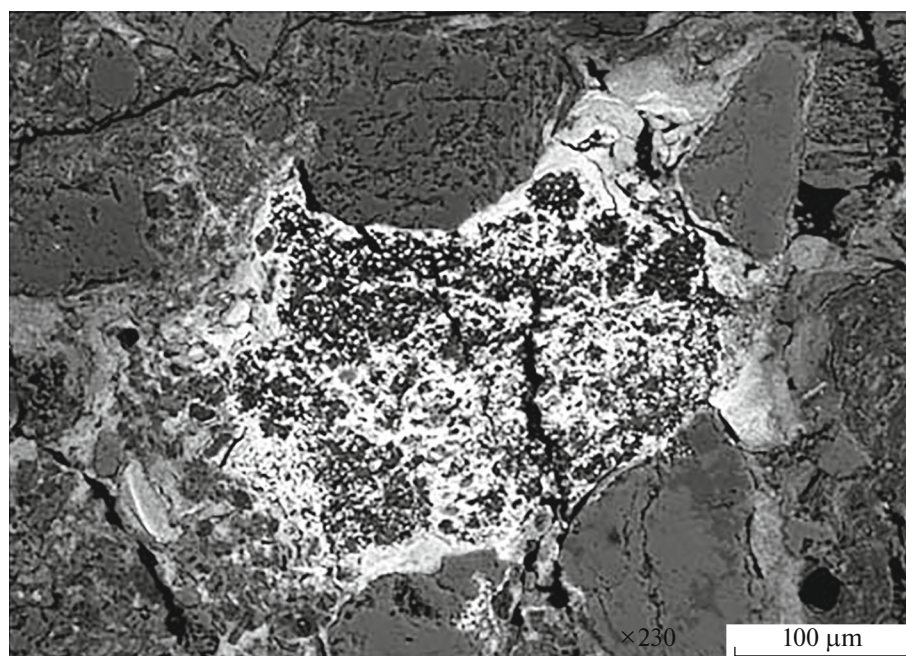


**Fig. 1.** Namaru deposit, sample 5461/316.4. Forms of segregations of Ca-phosphate of tetravalent uranium (white) in rocks of terrigenous sequence. BSE image.

When preparing samples for subsequent isotope studies, the following procedure was used. Sample decomposition was carried out in a slowly boiling solution with a mixture of concentrated HF and HNO<sub>3</sub> in a 5 : 1 ratio. Three aliquots were taken from the resulting solution: 1, to determine of U and Pb contents by the isotope dilution method using the mixed spike <sup>235</sup>U + <sup>208</sup>Pb; 2, to measure the isotopic composition of the common Pb and the <sup>234</sup>U/<sup>238</sup>U ratio; (3) to measure with high accuracy the <sup>238</sup>U/<sup>235</sup>U using the double spike <sup>236</sup>U + <sup>233</sup>U. In the aliquots for determining the U and Pb contents and <sup>238</sup>U/<sup>235</sup>U ratio, spikes were added prior to chromatographic separation of the elements. For mass spectrometry analysis, the studied elements were separated by ion exchange chromatography on a BioRad®AG 1 × 8 anion exchange resin with a 200–400 mesh. The total laboratory blank level during chemical preparation of samples did not exceed 0.1 ng for Pb and 0.02 ng for U.

Isotope studies were carried out at the Laboratory of Isotope Geochemistry and Geochronology, IGEM RAS. Isotope analysis of uranium and lead diluted with the mixed spike <sup>235</sup>U + <sup>208</sup>Pb, as well as common lead, was performed on a Micromass Sector 54 thermoionization 7-collector mass spectrometer. For uranium, the three-strip mode of an ion source with two tantalum evaporators and a rhenium ionizer was used. The isotopic composition of lead was analyzed in a single-strip mode with a silica gel activator on a rhenium substrate. The accuracy of the results of mass spectrometric measurements was controlled accord-

ing to the analysis of the International Standard Samples NIST Pb (SRM 981) and U (U 500). The instrumental mass discrimination coefficient, to which the results of the analyzes of the samples were corrected, was 1.0008 per unit difference in the masses of lead isotopes. In geochronological calculations, we used the generally accepted values of the decay constants of uranium (Steiger and Jager, 1977) and values <sup>238</sup>U/<sup>235</sup>U of our samples, obtained as a result of this study.

The isotopic composition of uranium was studied by multicollector inductively coupled plasma mass spectrometry (MC-ICP-MS) on a NEPTUNE (ThermoFinnigan). The analysis was carried out from solutions containing uranium, chromatographically separated from matrix elements of samples. The <sup>238</sup>U/<sup>235</sup>U ratio was measured with the double isotope spike <sup>233</sup>U + <sup>236</sup>U to correct the measurement results for mass-bias (Stirling et al., 2007). The <sup>234</sup>U/<sup>238</sup>U ratio, which does not require a double spike, was measured from a separate (untraced) aliquot of the sample. The specific isotope analysis methods used in this work were previously described in detail by us in (Chernyshev et al., 2014b).

## RESULTS

Sampling studies were carried out using samples from boreholes 5455, 5461 and 5468, characterizing the cross section of the ore body in its widest part close to junction of two paleovalleys (Fig. 2). The orebody is formed by several layers of bedded oxidation, which

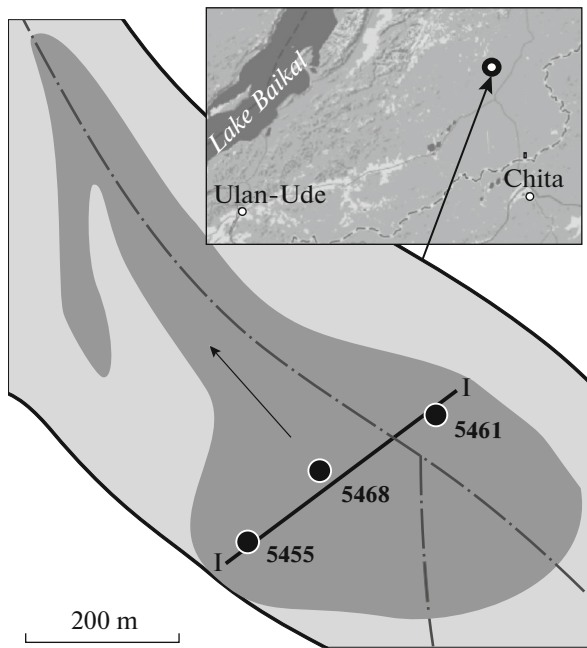


**Fig. 2.** Namaru deposit. Geological sketch of fragment of uranium ore body no. 5. Shades of gray show different U contents in metro percentages: dark gray,  $\geq 0.075$ ; light gray,  $< 0.075$ . Black circles show position of boreholes from which core samples were taken. I–I, line of section. Dash-dotted line marks axial lines of paleovalleys. Arrow shows direction of the descent of paleovalley slope. Dotted line in inset is administrative border of Republic of Buryatia and Zabaykalsky krai.

developed laterally, one above the other. The vertical section (Fig. 3) exposes alternating zones with different U content. The host rocks in most samples from borehole nos. 5455 and 5461 are represented by sand, the color of which varies from gray and greenish gray. In all samples from borehole no. 5468, as well as nos. 3 and 13, the host rocks are represented by silt and sandy carbonaceous silt.

The absolute heights of the boundary between the rocks of the Dzhilinda Formation and the basement rocks in borehole no. 5461, 5468 and 5455 are at 896.2, 896.3 and 886.5 m, and with overlying basalts, at 920.6, 912.9 and 904.2 m, respectively. According to XRD data, the main minerals in all studied samples are quartz, albite, and microcline. Calcite, dolomite, illite, and 7 Å-halloysite have also been noted. The chemical composition of the samples, according to XRF analysis, varies over a wide range (Tables 1 and 2). The most significant variations in the main rock-forming elements (Si and Al) are recognized on the flanks of the body. Good correlation between the  $Al_2O_3$  contents and loss on ignition (LOI) in the studied borehole intervals (Fig. 4) give reason to consider that these changes are mainly due to variations in the clay content in the samples. In sample no. 13 with the highest U content (7657  $\mu\text{g/g}$ ), the P, S, Ni, Rb, and Zr contents are several times higher, and for Zn it is almost 1.5 orders of value higher than in the other samples (see Table 2). The high level of mineralization in this sample can be explained by the increased

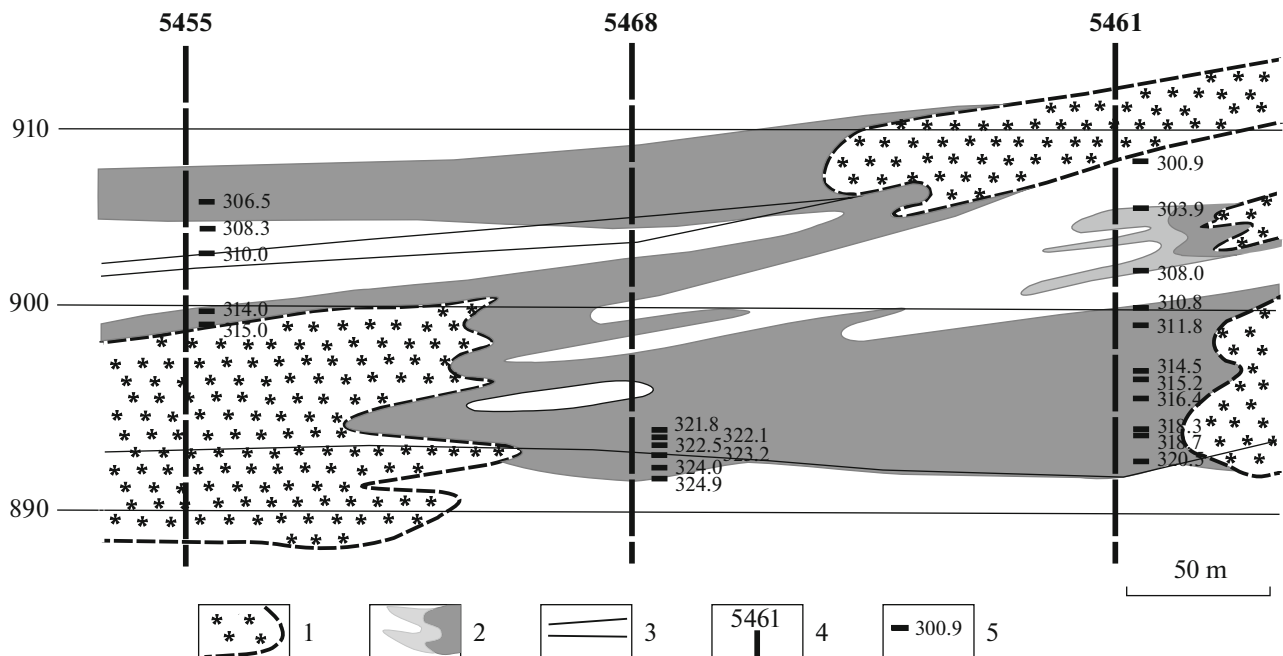


**Fig. 3.** Namaru deposit. Cross section of uranium ore body no. 5 along line I–I. (1) oxidation zone (reduced) and its boundary with initially gray-colored rocks; (2) ore bodies: shades of gray reflect different U contents in metro percentages: dark gray  $\geq 0.075$ ; light gray,  $< 0.075$ ; (3) lithological boundaries; (4) boreholes and their numbers; (5) sampling sites and depths from surface.

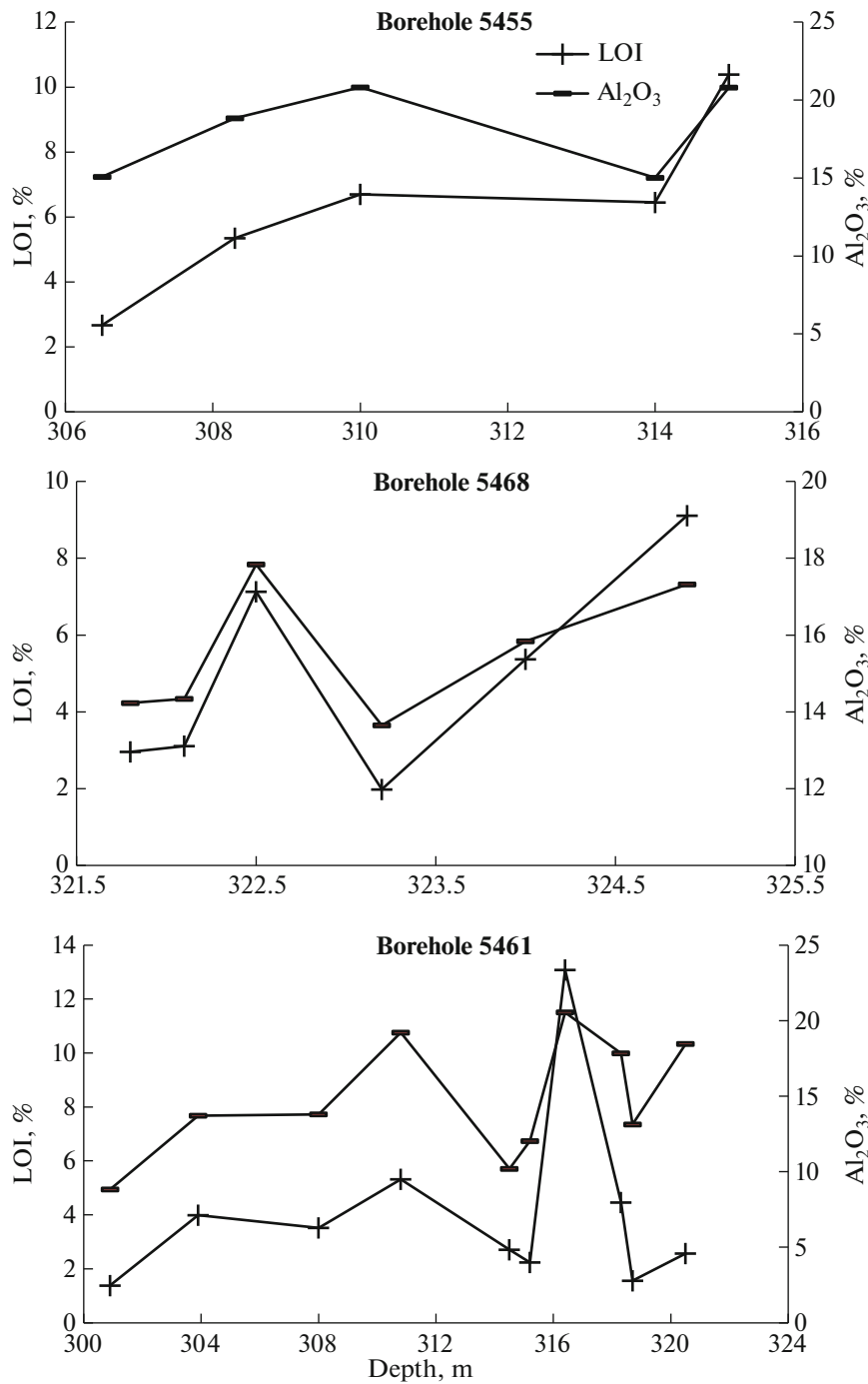


Fig. 4. Variations of Al<sub>2</sub>O<sub>3</sub> content and LOI value in ore interval of borehole nos. 5461, 5468, and 5455.

organic matter content and significant proportion of mafic volcanic ash.

Isotopic studies were aimed at obtaining data to estimate the behavior of uranium in various zones of the vertical and cross sections (see Figs. 3, 2) of ore body no. 5 of the Namaru deposit. For all selected samples, in addition to measuring the isotopic composition of uranium, we studied their U–Pb isotope systems (Table 3).

In the tables and plots, the measured <sup>238</sup>U/<sup>235</sup>U and <sup>234</sup>U/<sup>238</sup>U ratios are additionally presented in arbitrary units of δ<sup>238</sup>U and K<sub>234/238</sub>, respectively:

$$\delta^{238}\text{U} = \left[ \frac{(\frac{238}{235}\text{U})_{\text{sample}}}{(\frac{238}{235}\text{U})_{\text{st}}} - 1 \right] \times 1000\text{‰},$$

$$K_{234/238} = \frac{(\frac{234}{238}\text{U})_{\text{sample}}}{(\frac{234}{238}\text{U})_{\text{eq}}},$$

**Table 1.** Chemical composition of samples from borehole nos. 5455, 5461 and 5468 Namaru deposit. Major elements

| No.                  | Sampling depth, m | Content, wt % |                   |      |                                |                  |                  |      |                  |      |                                |                               |       |                  |                 |
|----------------------|-------------------|---------------|-------------------|------|--------------------------------|------------------|------------------|------|------------------|------|--------------------------------|-------------------------------|-------|------------------|-----------------|
|                      |                   | LOI           | Na <sub>2</sub> O | MgO  | Al <sub>2</sub> O <sub>3</sub> | SiO <sub>2</sub> | K <sub>2</sub> O | CaO  | TiO <sub>2</sub> | FeO  | Fe <sub>2</sub> O <sub>3</sub> | P <sub>2</sub> O <sub>5</sub> | S     | C <sub>org</sub> | CO <sub>2</sub> |
| <i>Borehole 5455</i> |                   |               |                   |      |                                |                  |                  |      |                  |      |                                |                               |       |                  |                 |
| 1                    | 306.5             | 2.67          | 2.18              | 0.33 | 15.08                          | 71.86            | 4.24             | 0.49 | 0.58             | 0.62 | 1.41                           | 0.31                          | 0.12  | n.d.             | 0.71            |
| 2                    | 308.3             | 5.35          | 0.92              | 0.79 | 18.84                          | 66.66            | 4.04             | 0.25 | 0.91             | 0.58 | 1.87                           | 0.04                          | 0.06  | 0.21             | 0.65            |
| 3                    | 310.0             | 6.70          | 1.01              | 0.82 | 20.82                          | 62.74            | 3.91             | 0.24 | 1.03             | 0.68 | 1.61                           | 0.04                          | 0.05  | 0.15             | 0.65            |
| 4                    | 314.0             | 6.45          | 0.57              | 0.38 | 15.02                          | 72.06            | 3.53             | 0.15 | 0.50             | 0.50 | 0.46                           | 0.04                          | 0.06  | n.d.             | 2.22            |
| 5                    | 315.0             | 10.39         | 0.62              | 0.47 | 20.81                          | 59.89            | 3.12             | 0.22 | 0.68             | n.d. | 3.42*                          | 0.05                          | 0.02  | n.d.             | n.d.            |
| <i>Borehole 5461</i> |                   |               |                   |      |                                |                  |                  |      |                  |      |                                |                               |       |                  |                 |
| 6                    | 300.9             | 0.71          | 1.45              | 0.17 | 9.10                           | 83.86            | 3.56             | 0.19 | 0.17             | 0.35 | 0.16                           | 0.03                          | 0.04  | n.d.             | 0.57            |
| 7                    | 303.9             | 3.99          | 2.10              | 0.20 | 13.71                          | 74.05            | 3.48             | 0.32 | 0.47             | 0.14 | 0.90                           | 0.03                          | 0.28  | n.d.             | n.d.            |
| 8                    | 308.0             | 3.52          | 1.55              | 0.23 | 13.80                          | 75.35            | 4.18             | 0.18 | 0.35             | 0.20 | 0.41                           | 0.02                          | 0.02  | 0.17             | 0.70            |
| 9                    | 310.8             | 6.52          | 2.13              | 0.33 | 19.21                          | 64.63            | 3.86             | 0.51 | 0.73             | 0.25 | 0.99                           | 0.11                          | 0.10  | n.d.             | n.d.            |
| 10                   | 311.8             | 1.01          | 1.40              | 0.17 | 8.47                           | 84.23            | 3.32             | 0.20 | 0.18             | 0.39 | 0.36                           | 0.03                          | 0.04  | n.d.             | n.d.            |
| 11                   | 314.5             | 2.71          | 1.69              | 0.23 | 10.19                          | 76.86            | 4.06             | 0.39 | 0.31             | 1.72 | 1.06                           | 0.04                          | <0.02 | n.d.             | 1.35            |
| 12                   | 315.2             | 2.24          | 2.18              | 0.16 | 12.03                          | 77.75            | 3.92             | 0.34 | 0.28             | 0.34 | 0.30                           | 0.08                          | 0.07  | n.d.             | n.d.            |
| 13                   | 316.4             | 13.08         | 1.03              | 0.47 | 20.55                          | 52.70            | 3.03             | 0.65 | 0.63             | n.d. | 1.31*                          | 0.81                          | 1.61  | 2.58             | 1.92            |
| 14                   | 318.3             | 4.46          | 1.55              | 0.33 | 17.84                          | 69.38            | 4.40             | 0.22 | 0.49             | 0.27 | 0.69                           | 0.04                          | <0.02 | n.d.             | 0.32            |
| 15                   | 318.7             | 1.56          | 3.57              | 0.08 | 13.13                          | 75.90            | 4.27             | 0.39 | 0.27             | 0.16 | 0.33                           | 0.08                          | <0.02 | n.d.             | n.d.            |
| 16                   | 320.5             | 2.57          | 2.41              | 0.15 | 18.46                          | 66.64            | 8.38             | 0.17 | 0.37             | 0.33 | 0.19                           | 0.04                          | <0.02 | n.d.             | 0.30            |
| <i>Borehole 5468</i> |                   |               |                   |      |                                |                  |                  |      |                  |      |                                |                               |       |                  |                 |
| 17                   | 321.8             | 2.96          | 1.40              | 0.39 | 14.23                          | 74.31            | 4.33             | 0.24 | 0.48             | 0.46 | 0.72                           | 0.07                          | 0.04  | n.d.             | 0.43            |
| 18                   | 322.1             | 3.11          | 2.01              | 0.39 | 14.34                          | 73.58            | 4.02             | 0.33 | 0.47             | 0.47 | 0.64                           | 0.10                          | 0.06  | n.d.             | 0.41            |
| 19                   | 322.5             | 7.13          | 1.05              | 0.58 | 17.84                          | 65.00            | 3.73             | 0.32 | 0.85             | 0.82 | 1.83                           | 0.10                          | 0.20  | 0.40             | 0.69            |
| 20                   | 323.2             | 1.98          | 2.81              | 0.25 | 13.65                          | 75.11            | 4.58             | 0.39 | 0.31             | 0.41 | 0.10                           | 0.08                          | 0.03  | n.d.             | 0.54            |
| 21                   | 324.0             | 5.37          | 1.51              | 0.73 | 15.84                          | 70.67            | 2.69             | 0.35 | 0.37             | 0.47 | 1.67                           | 0.06                          | 0.03  | n.d.             | 0.25            |
| 22                   | 324.9             | 9.11          | 0.82              | 0.78 | 17.32                          | 65.72            | 2.64             | 0.37 | 0.21             | 0.49 | 2.09                           | 0.09                          | <0.02 | n.d.             | 0.29            |



**Table 2.** Chemical composition of samples from borehole nos. 5455, 5461, and 5468 of Namaru deposit. Trace elements

| No.                  | Sampling depth, m | Content, µg/g |     |     |     |     |       |     |     |     |     |      | U  | Th | Pb |
|----------------------|-------------------|---------------|-----|-----|-----|-----|-------|-----|-----|-----|-----|------|----|----|----|
|                      |                   | Cr            | V   | Co  | Ni  | Cu  | Zn    | Rb  | Sr  | Zr  | Ba  |      |    |    |    |
| <i>Borehole 5455</i> |                   |               |     |     |     |     |       |     |     |     |     |      |    |    |    |
| 1                    | 306.5             | 21            | 55  | 23  | 55  | 88  | 62    | 162 | 168 | 267 | 647 | 2950 | <5 | 69 |    |
| 2                    | 308.3             | 31            | 123 | 15  | 27  | 35  | 59    | 164 | 102 | 310 | 633 | 40   | 14 | 27 |    |
| 3                    | 310.0             | 42            | 147 | 10  | 19  | 70  | 61    | 169 | 104 | 244 | 638 | 76   | 14 | 26 |    |
| 4                    | 314.0             | 21            | 86  | 10  | 15  | 17  | 331   | 165 | 60  | 208 | 437 | 110  | 13 | 32 |    |
| 5                    | 315.0             | 25            | 88  | 46  | 50  | 32  | 60    | 151 | 76  | 458 | 501 | 401  | 29 | 49 |    |
| <i>Borehole 5461</i> |                   |               |     |     |     |     |       |     |     |     |     |      |    |    |    |
| 6                    | 300.9             | <5            | 14  | <5  | <5  | <5  | 34    | 131 | 96  | 86  | 585 | 34   | <5 | 10 |    |
| 7                    | 303.9             | 14            | 64  | 308 | 84  | 27  | 102   | 159 | 127 | 183 | 657 | 138  | 16 | 33 |    |
| 8                    | 308.0             | 14            | 54  | 12  | 6   | 8   | 70    | 217 | 60  | 169 | 377 | 83   | 14 | 25 |    |
| 9                    | 310.8             | 16            | 98  | 23  | 34  | 8   | 61    | 212 | 124 | 407 | 531 | 1297 | 22 | 45 |    |
| 10                   | 311.8             | 10            | 17  | <5  | <5  | <5  | 48    | 145 | 91  | 87  | 552 | 98   | <5 | 16 |    |
| 11                   | 314.5             | 33            | 39  | 11  | 6   | 14  | 72    | 170 | 119 | 124 | 580 | 81   | <5 | 15 |    |
| 12                   | 315.2             | <5            | 29  | 13  | 12  | 16  | 67    | 176 | 136 | 220 | 539 | 1045 | 10 | 35 |    |
| 13                   | 316.4             | 32            | 115 | 292 | 354 | 24  | 12334 | 328 | 263 | 968 | 616 | 7657 | 21 | 80 |    |
| 14                   | 318.3             | 14            | 50  | 15  | 8   | 119 | 78    | 215 | 103 | 281 | 675 | 258  | 22 | 31 |    |
| 15                   | 318.7             | <5            | 18  | <5  | <5  | <5  | 24    | 186 | 192 | 265 | 806 | 1221 | <5 | 30 |    |
| 16                   | 320.5             | <5            | 29  | <5  | 5   | 15  | 16    | 293 | 108 | 495 | 519 | 165  | 30 | 30 |    |
| <i>Borehole 5468</i> |                   |               |     |     |     |     |       |     |     |     |     |      |    |    |    |
| 17                   | 321.8             | 17            | 44  | <5  | 11  | 84  | 69    | 157 | 108 | 280 | 671 | 540  | <5 | 22 |    |
| 18                   | 322.1             | 23            | 42  | 19  | 27  | 133 | 92    | 168 | 131 | 283 | 634 | 1151 | 14 | 29 |    |
| 19                   | 322.5             | 38            | 106 | 45  | 76  | 67  | 164   | 181 | 111 | 544 | 510 | 943  | 14 | 58 |    |
| 20                   | 323.2             | <5            | 20  | <5  | <5  | <5  | 19    | 140 | 106 | 304 | 360 | 595  | <5 | 28 |    |
| 21                   | 324.0             | <5            | 87  | <5  | <5  | <5  | 32    | 96  | 88  | 233 | 280 | 225  | 27 | 17 |    |
| 22                   | 324.9             | <5            | 82  | <5  | 11  | <5  | 41    | 124 | 85  | 230 | 299 | 1011 | 22 | 43 |    |

where  $(^{238}\text{U}/^{235}\text{U})_{\text{sample}}$  and  $(^{234}\text{U}/^{238}\text{U})_{\text{sample}}$  are the measured isotope ratios in the sample;  $(^{238}\text{U}/^{235}\text{U})_{\text{st}}$  is the  $^{238}\text{U}/^{235}\text{U}$  ratio in the CRM-112A standard sample, taken from the data of (Richter et al., 2010) and equal to  $137.837 \pm 0.015$ ;  $(^{234}\text{U}/^{238}\text{U})_{\text{eq}}$  is the ratio corresponding to the secular equilibrium  $^{234}\text{U}$  and  $^{238}\text{U}$  and equal to  $(5.497 \pm 0.019) \times 10^{-5}$  (Cheng et al., 2013).

Considering the results, we note that the values of the U–Pb isotopic age of the samples have a large error, since they contain a significant amount of common lead impurity. Even in the sample with the maximum uranium content (no. 13), the proportion of  $^{206}\text{Pb}$  impurity of the total  $^{206}\text{Pb}$  was about 60%, and the  $^{207}\text{Pb}$  impurity in the total  $^{207}\text{Pb}$  – 97.3%. In samples with a low uranium content (about 40 ng/g), the proportion of  $^{206}\text{Pb}$  impurity reached 97.2%, for  $^{207}\text{Pb}$ , 99.96%. Under these conditions, calculation of the concentrations of radiogenic  $^{206}\text{Pb}$  and  $^{207}\text{Pb}$  and

the U–Pb-age values from separated samples are especially critical to the isotopic composition of lead used in the calculations, which is introduced as a correction for common lead.

Correction for the isotopic composition of lead or lead-bearing mineral phases directly from the studied samples would be sufficiently correct, but such phases were not found in any of the samples. Therefore, corrections for common lead were carried out in accordance with the model values of (Stacey and Kramers, 1975). The real isotopic composition of common lead in different samples may differ somewhat, in particular, due to the heterogeneity of the composition of the ore-bearing sequence. For samples with a low uranium content, even relatively small differences in the isotopic composition of common lead from that adopted in the calculations of the isotopic age (about 0.02% for the  $^{207}\text{Pb}/^{204}\text{Pb}$  ratio) lead to a change in the age  $T$  ( $^{207}\text{Pb}/^{235}\text{U}$ ) by several million years. Given the latter circumstance, the data in Table 3 for  $T$  ( $^{207}\text{Pb}/^{235}\text{U}$ )

**Table 3.** Results of isotopic U–Pb,  $^{238}\text{U}$ – $^{234}\text{U}$  and  $^{238}\text{U}$ – $^{235}\text{U}$  study for samples from borehole nos. 5455, 5461, and 5468 of Namaru deposit

| No.                  | Sampling depth, m | $^{238}\text{U}/^{235}\text{U}$ | $\delta^{238}\text{U}$ ,<br>‰ | $^{234}\text{U}/^{238}\text{U}$<br>( $\times 10^5$ ) | $K_{234/238}$ | $^{206}\text{Pb}/^{204}\text{Pb}$ | T<br>( $^{206}\text{Pb}/^{238}\text{U}$ ),<br>Ma | T<br>( $^{207}\text{Pb}/^{235}\text{U}$ ),<br>Ma |
|----------------------|-------------------|---------------------------------|-------------------------------|--|---------------|-----------------------------------|--|--|
| <i>Borehole 5455</i> |                   |                                 |                               |  |               |                                   |  |  |
| 1                    | 306.5             | 137.649                         | -1.36                         | 6.68   | 1.215         | 21.85                             | 8.0  | (8.8)  |
| 2                    | 308.3             | 137.683                         | -1.12                         | 5.53   | 1.006         | 18.99                             | 26.1   | (7.6)  |
| 3                    | 310.0             | 137.691                         | -1.06                         | 5.48   | 0.997         | 19.21                             | 22.4   | (72.3)   |
| 4                    | 314.0             | 137.699                         | -1.00                         | 3.85   | 0.700         | 19.17                             | 19.8   | (10.5)   |
| 5                    | 315.0             | 137.799                         | -0.28                         | 7.55   | 1.373         | 19.38                             | 8.1  | (9.6)  |
| <i>Borehole 5461</i> |                   |                                 |                               |  |               |                                   |  |  |
| 6                    | 300.9             | 137.651                         | -1.35                         | 5.80   | 1.056         | 18.82                             | 12.4   | (6.9)  |
| 7                    | 303.9             | 137.598                         | -1.73                         | 6.82   | 1.241         | 19.53                             | 21.5   | (18.5)   |
| 8                    | 308.0             | 137.592                         | -1.78                         | 4.62   | 0.840         | 19.10                             | 17.3   | (21.0)   |
| 9                    | 310.8             | 137.484                         | -2.56                         | 7.32   | 1.332         | 21.54                             | 6.7  | (5.9)  |
| 10                   | 311.8             | 137.514                         | -2.34                         | 5.01   | 0.911         | 19.06                             | 9.3  | (9.0)  |
| 11                   | 314.5             | 137.523                         | -2.28                         | 5.37   | 0.977         | 19.18                             | 18.4   | (22.9)   |
| 12                   | 315.2             | 137.707                         | -0.94                         | 6.06   | 1.103         | 25.79                             | 13.4   | (10.6)   |
| 13                   | 316.4             | 137.688                         | -1.08                         | 5.78   | 1.051         | 31.32                             | 8.0  | (8.1)  |
| 14                   | 318.3             | 137.797                         | -0.29                         | 7.00   | 1.273         | 20.59                             | 12.1   | (6.6)  |
| 15                   | 318.7             | 137.742                         | -0.69                         | 8.41   | 1.529         | 21.37                             | 10.5   | (7.8)  |
| 16                   | 320.5             | 137.778                         | -0.43                         | 2.62   | 0.477         | 19.25                             | 6.6  | (3.2)  |
| <i>Borehole 5468</i> |                   |                                 |                               |  |               |                                   |  |  |
| 17                   | 321.8             | 137.770                         | -0.49                         | 4.82   | 0.877         | 21.97                             | 12.7   | (13.3)   |
| 18                   | 322.1             | 137.730                         | -0.78                         | 5.08   | 0.924         | 23.44                             | 10.8   | (11.1)   |
| 19                   | 322.5             | 137.786                         | -0.37                         | 5.70   | 1.037         | 22.52                             | 19.6   | (20.7)   |
| 20                   | 323.2             | 137.836                         | -0.01                         | 3.61   | 0.657         | 20.61                             | 10.4   | (12.0)   |
| 21                   | 324.0             | 137.851                         | 0.10                          | 5.29   | 0.963         | 20.12                             | 13.2   | (8.5)  |
| 22                   | 324.9             | 137.833                         | -0.03                         | 8.19   | 1.489         | 20.26                             | 7.1  | (4.9)  |

are considered only to assess the degree of discordance of the values of U–Pb–age, which is determined by the difference between the values of T ( $^{206}\text{Pb}/^{238}\text{U}$ ) and T ( $^{207}\text{Pb}/^{235}\text{U}$ ) divided by the average of these two values.

## DISCUSSION

Comparison of the direction of the **change** in uranium content and  $^{206}\text{Pb}/^{204}\text{Pb}$  ratio in successive series of samples from the ore intervals of the studied boreholes showed good agreement of these characteristics for most samples (Fig. 5). Taking into account the relatively young age of uranium mineralization (about 12 Ma, Golubev et al., 2013), this agreement, gives reason to consider that the ore body mainly preserved the outlines acquired at the early stage of its formation. At the same time, the U–Pb isotopic age values of samples selected from different boreholes and at dif-

ferent levels of the vertical section span a wide range (see Table 3).

For almost half the samples, the obtained age values are significantly higher than 12 Ma. The largest scatter (from 12.4 to 26.1 Ma) was established for samples with a low (no more than 40  $\mu\text{g}/\text{g}$ ) uranium content. For samples with a high uranium content and degree of age discordance of no more than 10%, the range of T values is much smaller, 8.0–10.8 Ma. A high degree of discordance in the age of a number of samples (several tens of percent) indicates the significant role of migration processes of the intermediate decay products in the series  $^{238}\text{U}$  (RD $^{238}\text{U}$ ). The results of measurement of the  $^{234}\text{U}/^{238}\text{U}$  ratio in the samples are another argument for RD $^{238}\text{U}$  migration within the section. For most samples, it differs from the equilibrium ratio of the contents of these isotopes (see Table 3). The reason is the weaker bond of  $^{234}\text{U}$  (as



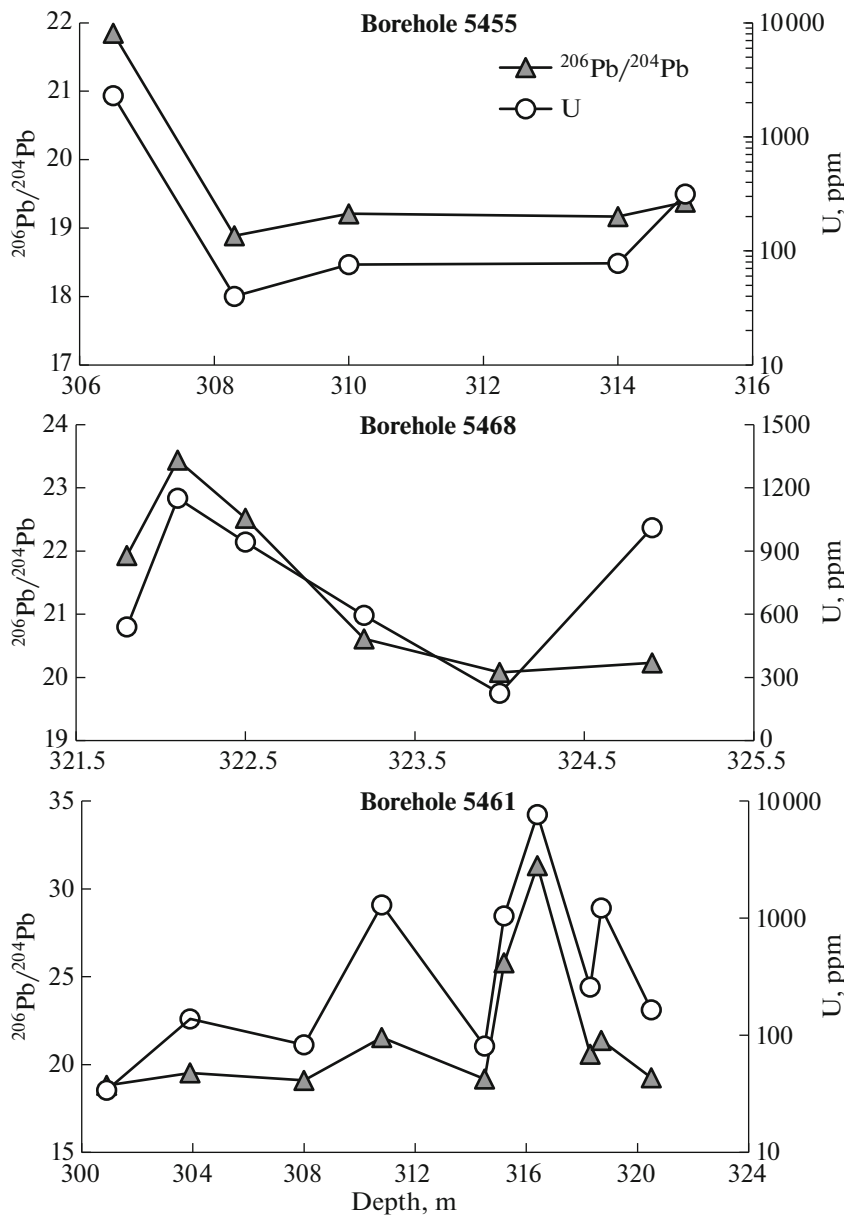


Fig. 5. Change in uranium content and  $^{206}\text{Pb}/^{204}\text{Pb}$  value in ore interval of borehole nos. 5461, 5468 and 5455.

a decay product) versus  $^{238}\text{U}$  in the rock when exposed to natural waters, more  $^{234}\text{U}$  than  $^{238}\text{U}$  passes into the aqueous phase, and as a result, the  $^{234}\text{U}/^{238}\text{U}$  ratio is disturbed (Thurber et al., 1962; Cherdynstev, 1971).

The difference of the measured  $^{234}\text{U}/^{238}\text{U}$  value in the samples from equilibrium is associated with both a deficit and excess of  $^{234}\text{U}$ . The deviation of the  $^{234}\text{U}/^{238}\text{U}$  ratio from the equilibrium value for most samples exceeds 5%. In the case when uranium-234 and common uranium migrated together, two models for the U-Pb isotope system are possible: (1)  $^{234}\text{U}$  deficit relative to equilibrium  $^{234}\text{U}/^{238}\text{U}$ . Then there will be an increase in the U-Pb age for the studied samples;

(2)  $^{234}\text{U}$  excess relative to equilibrium  $^{234}\text{U}/^{238}\text{U}$ . Then there will be a decrease in the U-Pb age. Such an isotopic age correlation is observed in sample nos. 3–5, 8, 9, 11, and 21 (see Table 3). However, in a number of samples with old U-Pb isotopic age (about 20 Ma), there is excess of  $^{234}\text{U}$  (sample nos. 2, 7, 12, and 19; see Table 3), and with low values (less than 8 Ma), – a deficit of  $^{234}\text{U}$  (sample no. 16; see Table 3).

Variations in the U-Pb ages and  $^{234}\text{U}/^{238}\text{U}$  ratios characteristic of the ore of the Namaru deposit indicate uranium migration that took place in the ore body of the deposit after its formation, and very likely to a change in the uranium concentrations. Let us consider possible scenarios of the processes that led to the

observed relations of the U–Pb–age values and the  $^{234}\text{U}/^{238}\text{U}$  ratio. The “ancient” U–Pb ages (ca. 20 Ma) recorded in some zones of the ore body, combined with excess  $^{234}\text{U}$ , are the result of two sequential and continuous processes: loss of common uranium and  $^{234}\text{U}$  input. The first process led to an increase in the Pb/U ratio in the ores and its U–Pb “aging”; the second, to an excess of  $^{234}\text{U}$ . The  $^{234}\text{U}$  excess shows that the process of its input, even if it ended, is no earlier than 1 Ma ago. To estimate the total duration of this process, the character of the discordance of the ages calculated from the  $^{206}\text{Pb}/^{238}\text{U}$  and  $^{207}\text{Pb}/^{235}\text{U}$  ratios is of key importance (see Table 3). In a significant part of the samples (7 out of 11), uranium is characterized by excess  $^{234}\text{U}$ ; the relation  $T(^{206}\text{Pb}/^{238}\text{U}) > T(^{207}\text{Pb}/^{235}\text{U})$  is observed, which is quite rare for the U–Pb geochronology. It indicates entry into the U–Pb geochronological system—which these samples represent—of a long-lived nuclide, a member of the radioactive family  $^{238}\text{U}$ , which in this case is  $^{234}\text{U}$ . So that the decay of  $^{234}\text{U}$  in turn could provide excess  $^{206}\text{Pb}$ , the input of  $^{234}\text{U}$  should have continued for a time commensurate with the determined age, in our case, several million years.

To explain the deficit of  $^{234}\text{U}$  in zones of the ore body with low U–Pb isotopic age (less than 8 Ma), it should be assumed that after the input of the common uranium that took place in the past, a young process of the loss of easily mobile  $^{234}\text{U}$  took place.

Young U–Pb ages (8.1 and 7.1 Ma) and high (1.37 and 1.49)  $K_{234/238}$  values in sample nos. 5 and 22 from the lower part of the section of borehole nos. 5455 and 5468 (see Table 3) indicate a recent (less than 1 Ma), possibly modern, contribution of the common uranium here. The sources of uranium were most likely the nearest zones of the ore deposit. The overlying rocks can be considered such sources, from which sample nos. 4 and 21 were collected (see Table 3). They have a deficit  $^{234}\text{U}$  and common uranium, as indicated by low (less than 1)  $K_{234/238}$  values and old U–Pb isotopic ages.

For sample. no. 16 from the lower part of the section of borehole no. 5461, just like for sample nos. 5 and 22, a young U–Pb age (6.5 Ma) was obtained, which may also indicate a relatively recent contribution of the common uranium. However, the  $K_{234/238}$  value is very low: 0.477. The deficit of  $^{234}\text{U}$  in this sample may be linked with the manifestation of inferred young hydrothermal event, which led, in particular, to an increase in the  $\text{K}_2\text{O}$  content of up to 8.38 in this zone, which is 1.8–3.1 times higher than in other samples from the studied section (see Table 1). In samples lying above (nos. 13–15), the  $K_{234/238}$  values are greater than 1, and the U–Pb ages (8.0, 10.4, and 12.1 Ma) are smaller less (sample nos. 13 and 15) or close (samples 14) to the age of the main phase of uranium mineralization in the KhOF (Golubev et al., 2013). A possible

source of excess  $^{234}\text{U}$  and common U in this part of the section could have been material from the underlying part of the terrigenous sequence, in which, as the results of studying sample no. 16 showed, there is a deficit of  $^{234}\text{U}$  and common U.

In other parts of the section, there are alternating zones with a deficit and excess of  $^{234}\text{U}$ . An increase in the  $^{234}\text{U}$  content with respect to the equilibrium  $^{234}\text{U}/^{238}\text{U}$  is not always accompanied by simultaneous input of common uranium and, accordingly, a decrease in the U–Pb age, and a deficit of  $^{234}\text{U}$  is not always accompanied by simultaneous removal of common uranium and an increase in the U–Pb age.

The  $^{238}\text{U}/^{235}\text{U}$  values obtained from the samples ranges from 137.484 to 137.851, or 2.66‰ (see Table 3). The heaviest uranium with  $\delta^{238}\text{U}$  values from  $-0.68$  to  $0.10$ ‰ (on average,  $-0.26$ ‰) is typical of samples from the central part of the section, in borehole no. 5468. In samples from borehole nos. 5455 and 5461, the  $\delta^{238}\text{U}$  values vary in a wider range: from  $-1.36$  to  $-0.28$ ‰ (average  $-0.96$ ‰) and from  $-2.56$  to  $-0.29$ ‰ (average  $-1.41$ ‰), respectively. Comparison of the variations in  $\delta^{238}\text{U}$  and uranium content in vertical sections of the studied boreholes (Fig. 6) shows that in boreholes nos. 5461 and 5468 the direction of variation of these two parameters from sample to sample is opposite (with the exception of the intervals 314.5–315.2 and 320.5–322.4 m in borehole no. 5461). This means that in most of the vertical section, with an increase in uranium content in the samples, there is a decrease in the fraction of heavy  $^{238}\text{U}$ . In the vertical section of borehole no. 5455, the direction of the change in  $\delta^{238}\text{U}$  and uranium content is the same only in the upper part of the section. In other areas of the borehole, the change in these values from sample to sample is different: with an increase in the uranium content in the samples, the proportion of heavy  $^{238}\text{U}$  (see Fig. 6). However, whereas in the lower part of the section this direction is very distinct, in the middle it is very weak. The nature of changes in the uranium content, U–Pb ages, and  $K_{234/238}$  values in the lower part of the cross section of borehole indicates the input of total uranium into this area (sample no. 5), the source of which can be considered the overlying rocks. This process is accompanied by enrichment in the heavy isotope  $^{238}\text{U}$  of the solid phase, which includes reduced uranium (Chernyshev et al., 2014a). Similar changes in uranium contents, U–Pb ages, and  $K_{234/238}$  are noted in the upper part of the section of borehole. 5455, but here the input of total uranium is accompanied by enrichment of the solid phase in the light isotope  $^{235}\text{U}$ . This direction of  $^{238}\text{U}$  and  $^{235}\text{U}$  fractionation may have the following explanations: (1) with successive deposition of the solid phase from the uranium-bearing solution, as it is exhausted, successive “lightening” of the isotopic composition of uranium occurs; (2) during replace-

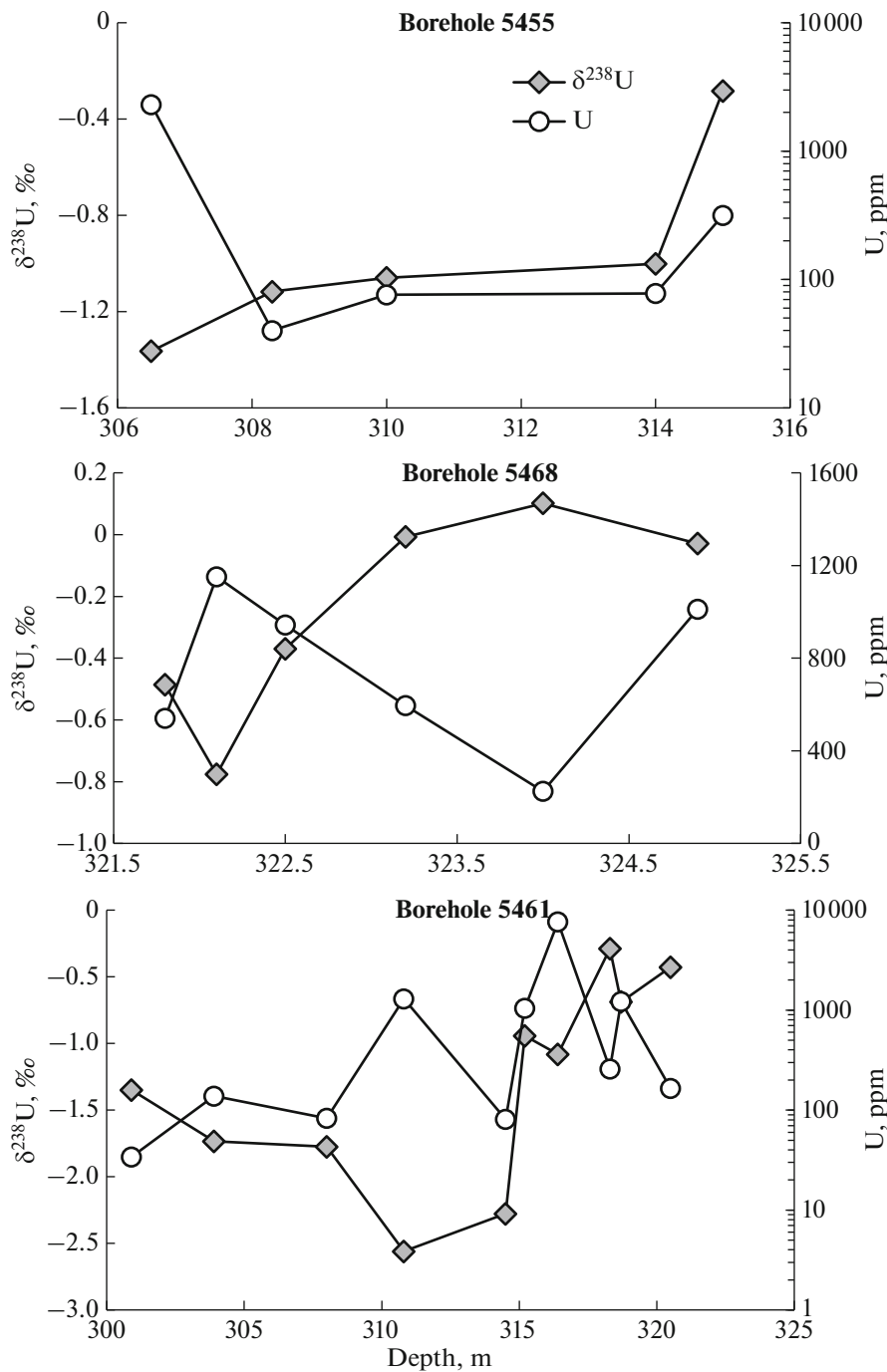


**Fig. 6.** Change in  $^{238}\text{U}/^{235}\text{U}$  ratio ( $\delta^{238}\text{U}$ ) and uranium content in ore interval of borehole nos. 5461, 5468 and 5455.

ment (dissolution) of the previously formed uranium phases, the isotopes  $^{238}\text{U}$  and  $^{235}\text{U}$  are fractionated, expressed as enrichment in the light isotope  $^{235}\text{U}$  of later mineral phases (solution).

The considered patterns for the change in the U–Pb,  $^{238}\text{U}$ – $^{234}\text{U}$ , and  $^{238}\text{U}$ – $^{235}\text{U}$  isotope systems in the ore interval of borehole no. 5455, also occur in some form in the ore intervals of borehole nos. 5461 and

5468. Note that in all zones of the section (in all boreholes) in the lower zone of the ore body, the content of the light isotope  $^{235}\text{U}$  is less than in the higher zone (Fig. 7). Depletion in the light isotope  $^{235}\text{U}$  of the lower zone of the deposit may be associated with the acting of ascending carbonic waters established in the basement of the region. In (Chernyshev et al., 2019), it was shown that the effect of such waters on uranium-

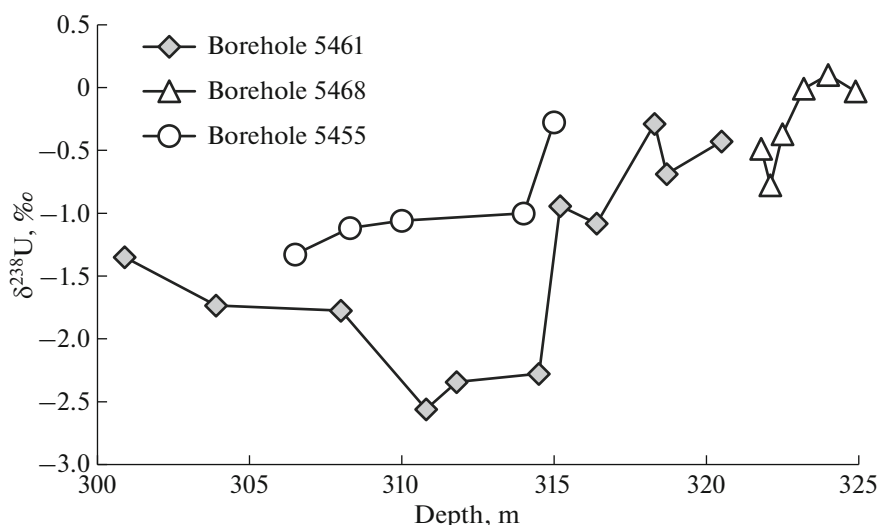


Fig. 7. Variation of  $\delta^{238}\text{U}$  in vertical section of ore interval in different zones of ore body no. 5.

bearing rocks leads to predominant leaching of the light isotope  $^{235}\text{U}$ .

## CONCLUSIONS

As a result of studying the U–Pb isotope systems and the isotopic composition of uranium ( $^{234}\text{U}/^{238}\text{U}$  and  $^{238}\text{U}/^{235}\text{U}$ ) of a set of samples taken in different zones of the vertical and cross sections of ore body no. 5 of the Namaru deposit, wide variations in the U–Pb isotopic age and isotopic composition of uranium were established. In all samples, the measured  $^{234}\text{U}/^{238}\text{U}$  ratio differs from the equilibrium value, which is associated with both a deficit and excess of  $^{234}\text{U}$  in the samples. The U–Pb ages of the samples range from 6.6 to 26.1 Ma. The smallest of the obtained values is significantly younger than the age of the main stage of uranium mineralization of the KhOF (ca. 12 Ma (Golubev et al., 2013)), and the maximum is 9 Ma older than the onset of deposition of rocks of the Dzhilinda Formation (Kochkin et al., 2017b) hosting the uranium mineralization. Variations in the U–Pb age and  $^{234}\text{U}/^{238}\text{U}$  ratio characteristic in the ores of the Namaru deposit indicate the uranium migration that took place in the ore body of the deposit after its formation, as well as a possible change in the uranium concentrations. Hence, it follows that the development of the permafrost layer that 2.5 Ma ago covered the catchment area of paleovalleys with meteoric oxygen-containing waters did not provide the expected (Kochkin et al., 2017b) conservation of uranium ores and U migration processes took place at the deposit, including during the Quaternary. This may be due to the possible reactivation of the hydrodynamic regime in the recent past during partial thawing of the permafrost zone (Paleoklimat..., 2009; Vaks et al., 2013).

In a number of samples with excess  $^{234}\text{U}$ , the  $T(^{206}\text{Pb}/^{238}\text{U})$  values are greater than the  $T(^{207}\text{Pb}/^{235}\text{U})$  values. This points to incoming of a long-lived nuclide, a member of the radioactive  $^{238}\text{U}$  family, which in this case is  $^{234}\text{U}$ . So that the decay of  $^{234}\text{U}$  could, in turn, provide excess radiogenic  $^{206}\text{Pb}$ , the input of  $^{234}\text{U}$  should have continued for a time commensurate with the determined age, in our case, over several million years.

The wide range of variations in the  $^{238}\text{U}/^{235}\text{U}$  ratio (137.484–137.851) in all parts of the studied profile can be explained by the different locations of the samples with respect to the ore deposition front and the change in redox conditions as this front advanced.. Significant depletion in the light isotope  $^{235}\text{U}$  in the lower zone of the ore body may be associated with the action of ascending carbonic waters established in the regional basement.

The study of the Namaru deposit, in addition with previously obtained data on the Dybryn field (Golubev et al., 2013), showed the effectiveness of combining U–Pb isotope dating and determinations of the isotopic composition of uranium ( $^{234}\text{U}/^{238}\text{U}$  and  $^{238}\text{U}/^{235}\text{U}$ ) to assess the post-ore redistribution of uranium: removal of uranium from some zones of the ore body and its concomitant redeposition in others.

## ACKNOWLEDGMENTS

The authors thank the reviewers for helpful comments.

## FUNDING

This work was financially supported by the State Research Program of Institute of Geology of Ore Deposits,

Petrography, Mineralogy and Geochemistry, Russian Academy of Sciences.

### CONFLICT OF INTEREST

The authors declare that they have no conflict of interest.

### OPEN ACCESS

This article is licensed under a Creative Commons Attribution 4.0 International License, which permits use, sharing, adaptation, distribution and reproduction in any medium or format, as long as you give appropriate credit to the original author(s) and the source, provide a link to the Creative Commons license, and indicate if changes were made. The images or other third party material in this article are included in the article's Creative Commons license, unless indicated otherwise in a credit line to the material. If material is not included in the article's Creative Commons license and your intended use is not permitted by statutory regulation or exceeds the permitted use, you will need to obtain permission directly from the copyright holder. To view a copy of this license, visit <http://creativecommons.org/licenses/by/4.0/>.

### REFERENCES

- Andersen, M.B., Stirling, C.H., and Weyer, S., Uranium isotope fractionation, *Rev. Mineral. Geochem.*, 2017, vol. 82, pp. 799–850.
- Basu, A., Brown, S.T., Christensen, J.N., DePaolo, D.J., Reimus, P.W., Heikoop, J.M., Woldegabriel, G., Simmons, A.M., House, B.M., Hartmann, M., and Maher, K., Isotopic and geochemical tracers for U(VI) reduction and U mobility at an in situ recovery U mine, *Environ. Sci. Technol.*, 2015, vol. 49, pp. 5939–5947.
- Cheng, H., Lawrence, E.R., Shen, C.C., Polyak, V.J., Asmerom, Y., Woodhead, J., Hellstrom, J., Wang, Y., Kong, X., Spotl, C., Wang, X., and Alexander, Jr. E.C., Improvements in  $^{230}\text{Th}$  dating,  $^{230}\text{Th}$  and  $^{234}\text{U}$  half-life values, and U–Th isotopic measurements by multi-collector inductively coupled plasma mass spectrometry, *Earth Planet. Sci. Lett.*, 2013, vol. 371–372, pp. 82–91.
- Cherdyntsev, V.V., *Uranium-234*, (Jerusalem, Israel Program for Scientific Translations, 1971).
- Chernyshev, I.V., Dubinina, E.O., and Golubev, V.N., Fractionation factor of  $^{238}\text{U}$  and  $^{235}\text{U}$  isotopes in the process of hydrothermal pitchblende formation: a numerical estimate, *Geol. Ore Deposits*, 2014a, vol. 56, no. 5, pp. 315–321.
- Chernyshev, I.V., Golubev, V.N., Chugaev, A.V., and Baranova, A.N.,  $^{238}\text{U}/^{235}\text{U}$  isotope ratio variations in minerals from hydrothermal uranium deposits, *Geochem. Int.*, 2014b, vol. 52, no. 12, pp. 1013–1029.
- Chernyshev, I.V., Golubev, V.N., Chugaev, A.V., Mandzheva, G.V., and Gareev, B.I., Behavior of the  $^{238}\text{U}$ ,  $^{235}\text{U}$ , and  $^{234}\text{U}$  isotopes at weathering of volcanic rocks with U mineralization: a case study at the Tulukuevskoe Deposit, Eastern Transbaikalia, *Petrology*, 2019, vol. 2, no. 4, pp. 407–424.
- Cuney, M. and Kyser, K., *Recent and not-so-recent developments in uranium deposits and implications for exploration*, *Short Course Series*, 2008, vol. 39.
- Golubev, V.N., Chernyshev, I.V., Chugaev, A.V., Eremina, A.V., Baranova, A.N., and Krupskaya, V.V., U–Pb systems and U isotopic composition of the sandstone-hosted paleovalley Dybryn uranium deposit, Vitim uranium district, Russia, *Geol. Ore Deposits*, 2013, vol. 55, no. 6, pp. 399–410.
- Kochkin, B.T., Solodov, I.N., Ganina, N.I., Rekun, M.L., Tarasov, N.N., Shugina, G.A., and Shulik, L.S., Geochemical features of the ore-bearing medium in uranium deposits in the Khiagda ore field, *Geol. Ore Deposits*, 2017a, vol. 59, no. 5, pp. 341–353.
- Kochkin, B.T., Tarasov, N.N., Andreeva, O.V., Asadulin, En.E., and Golubev, V.N., Polygenetic and polychronic uranium mineralization at deposits of the Khiagda ore field, Buryatia, *Geol. Ore Deposits*, 2017b, vol. 59, no. 2, pp. 141–155.
- Kochkin, B.T., Tarasov, N.N., Velichkin, V.I., Nesterova, M.V., Novgorodtsev, A.A., and Shulik, L.S., Iron redistribution during postore stage at uranium deposits of the Khiagda ore field, Vitim District, *Geol. Ore Deposits*, 2014, vol. 56, no. 2, pp. 113–127.
- Mashkovtsev, G.A., Konstantinov, A.K., Miguta, A.K., Shumilin, M.V., and Shchetochkin, V.N., *Uran rossiskikh neдр* (Uranium of the Russian Interiors), Moscow: VIMS, 2010.
- Murthy, M.J., Stirling, C.H., Kaltenbach, A., Turner, S.P., and Schaefer, B.F., Fractionation of  $^{238}\text{U}/^{235}\text{U}$  by reduction during low temperature uranium mineralization processes, *Earth Planet. Sci. Lett.*, 2014, vol. 388, pp. 306–317.
- Paleoklimat i paleolandshafty vnetropicheskogo prostranstva Severnogo polushariya. Pozdnyy pleistotsengolotsen. Atlas—monografiya* (Paleoclimate and Paleolandscale of the Extratropical Space of the Northern Hemisphere. Late Pleistocene—Holocene. Atlas—Monograph), Moscow: GEOS, 2009.
- Placzek, C.J., Heikoop, J.M., House, B., Linhoff, B.S., and Pelizza, M., Uranium isotope composition of waters from South Texas uranium ore deposits, *Chem. Geol.*, 2016, vol. 437, pp. 44–55.
- Richter, S., Eykens, R., Kuhn, H., Kohn, H., Aregbe, Y., Verbruggen, A., and Weyer, S., New average values for the  $n(^{238}\text{U})/n(^{235}\text{U})$  isotope ratios of natural uranium standards, *Int. J. Mass Spectrom.*, 2010, vol. 295, pp. 94–97.
- Stacey, J.S. and Kramers, I.D., Approximation of terrestrial lead isotope evolution by a two-stage model, *Earth Planet. Sci. Lett.*, 1975, vol. 26, pp. 207–221.
- Steiger, R.H. and Jager, E., Subcommittee on geochronology: convention on the use of decay constants in geo- and cosmochronology, *Earth Planet. Sci. Lett.*, 1977, vol. 36, pp. 359–362.
- Stirling, C.H., Andersen, M.B., Potter, E.K., and Halliday, A.N., Low-temperature isotopic fractionation of uranium, *Earth Planet. Sci. Lett.*, 2007, vol. 264, pp. 208–225.
- Svyatetskii, V.S., Polonyankina, S.V., and Ermakov, A.G., Uranium mining extraction of Russia: state and prospects of development, *Razved. Okhr. Nedr*, 2017, no. 12, pp. 22–26.
- Thurber, D.L., Anomalous  $^{234}\text{U}/^{238}\text{U}$  in nature, *J. Geophys. Res.*, 1962, vol. 67, pp. 4518–4520.
- Vaks, A., Gutareva, O.S., Breitenbach, S.F.M., Avirmed, E., Mason, A.J., Thomas, A.L., Osinzev, A.V., Kononov, A.M., and Henderson, G.M., Speleothems reveal 500,000-year history of Siberian permafrost, *Science*, 2013, vol. 340, no. 6129, pp. 183–186.
- Zhivov, V.L., Boitsov, A.V., and Shumilin, M.V., *Uran: geologiya, dobycha, ekonomika* (Uranium: Geology, Mining and Economics), Moscow: OAO “Atomredmetzoloto”, 2012.